org. Helmholtz Association (ar-410296) IP: 134.94.123.71 On: Mon, 10 Aug 2026 17:14:48

ANNUAL REVIEWS

Annual Review of Materials Research

Electroplasticity of Metals and Ceramics: Current Status

Apurv Dash,[1,2] Yu-chen Liu,[3,4] Hidehiro Yoshida,[5,6] Robert Mücke,[1] Gregory Gerstein,[7] Sebastian Herbst,[7] Florian Nürnberger,[7] Hans Jürgen Maier,[7] Heung Nam Han,[8] Shih-kang Lin,[3,9,10] and Olivier Guillon[1,11]

[1]Materials Synthesis and Processing (IMD-2), Institute of Energy Materials and Devices, Jülich, Germany; email: o.guillon@fz-juelich.de

[2]Department of Energy Conversion and Storage, Technical University of Denmark, Lyngby, Denmark

[3]Department of Materials Science and Engineering, National Cheng Kung University, Tainan City, Taiwan

[4]Department of Mechanical Engineering, National Cheng Kung University, Tainan City, Taiwan

[5]Department of Materials Science and Engineering, School of Engineering, The University of Tokyo, Tokyo, Japan

[6]Next Generation Zirconia Social Cooperation Program, Institute of Engineering Innovation, School of Engineering, The University of Tokyo, Tokyo, Japan

[7]Institut für Werkstoffkunde (Materials Science), Leibniz University Hannover, Garbsen, Germany

[8]Department of Materials Science and Engineering and Research Institute of Advanced Materials, Seoul National University, Seoul, Republic of Korea

[9]Program on Smart and Sustainable Manufacturing, Academy of Innovative Semiconductor and Sustainable Manufacturing, National Cheng Kung University, Tainan City, Taiwan

[10]Hierarchical Green-Energy Materials (Hi-GEM) Research Center, National Cheng Kung University, Tainan City, Taiwan

[11]Jülich Aachen Research Alliance (JARA-Energy), Jülich, Germany

ANNUAL REVIEWS CONNECT

www.annualreviews.org

- Download figures
- Navigate cited references
- Keyword search
- Explore related articles
- Share via email or social media

Annu. Rev. Mater. Res. 2025. 55:151–74

First published as a Review in Advance on April 10, 2025

The *Annual Review of Materials Research* is online at matsci.annualreviews.org

https://doi.org/10.1146/annurev-matsci-081720-111526

Copyright © 2025 by the author(s). This work is licensed under a Creative Commons Attribution 4.0 International License, which permits unrestricted use, distribution, and reproduction in any medium, provided the original author and source are credited. See credit lines of images or other third-party material in this article for license information.

OPEN ACCESS CC BY

Keywords

electroplasticity, flash, dislocation, grain boundary sliding, defects

Abstract

This review covers the anelastic deformation observed under electric loading (electroplasticity) of metals and ceramics. The interplay of various complex mechanisms beyond trivial Joule heating leading to enhanced plasticity is discussed in the context of both materials classes. In the case of metals, electromechanical coupling resulting in forces being exerted on atoms and dislocations is elucidated. In the case of ceramics, change in the grain boundary structure is proposed to justify the enhanced plasticity. Microstructural evidence is analyzed in correlation with the deformation behavior.

Downloaded from www.annualreviews.org. Helmholtz Association (ar-410296) IP: 134.94.123.71 On: Mon, 10 Aug 2026 17:14:48

1. INTRODUCTION

The shaping of materials with technological importance has led in part to the present state of human civilization. Usually, temperature and mechanical stress are sufficient to induce deformation; however, ceramics and certain metals are brittle and have limitations to deformation even at both high temperatures and high pressures. Thus, electric field– and current–assisted deformation comes as a boon to the engineers and scientists interested in shaping ceramics, such as zirconia and alumina, and metals, such as tungsten and magnesium (1–4). The possibility of deformation-based shaping of these brittle materials can further push the current state of technological advancement in the field of materials science.

It has been twenty-five years since the exhaustive review of the electroplasticity of ceramics and metals by Hans Conrad (1). The present article is an effort to review recent works on electroplasticity, including from a microstructure point of view. Depending on the deformation scheme, the process of electroplasticity is categorized as creep, which takes place under a constant stress level for a longer period, or superplastic deformation, which is a high-strain-rate deformation.

This review presents the latest understanding of the electroplasticity of metals and ceramics, dealing with the determination of physical quantities that react sensitively to electric loading and estimating the magnitude of this change. This comparison between two classes of materials with different properties enables us to identify similarities but also highlights differences and helps predict the behavior of metal–ceramic composites.

2. ELECTROPLASTICITY IN METALS

2.1. Behavior

The chronological study of the electroplastic effect (EPE) can be roughly divided into three periods:

1. The period of the discovery of electroplasticity and development of different theories explaining the effect occurred from 1963 when Troitskii & Likhtman published their first paper (5) to 2000 when Conrad published his last fundamental paper (1).
2. A period of intense publication of papers on electrical pulse processing with low ($<$2,000 A/mm^2) current densities ran from 2000 to 2017. Such publications appear in large numbers up to the present day (6).
3. Finally, 2017 and on saw the creation of new physical models of current impact, the interaction between electric current and microstructural elements, in situ studies, methods for creating composites based on electroplasticity (7), and the start of industrial application of EPE-based technologies (6, 8). In particular, mechanical aspects such as yield stress, stress relaxation, creep deformation, generation of dislocations and dislocation mobility, material fatigue, and metal forming were examined. High current densities were used to increase the effect of the drift electrons, while short pulse durations were used to minimize sample heating (9, 10). In contrast to macroscopic experiments with high current densities, various studies have examined the reduction in microhardness when using low current densities (11, 12).

In this section, we first review microstructure evolution involving defect dynamics in metals under current loading. Much experimental evidence has been gathered in the literature, and a few examples are presented in **Figure 1**. **Figure 1*a*** shows a high population of jagged dislocations, the so-called wavy slip, found in Ti-6Al under a pulsed current with 5% mechanical strain (13). This pattern was different from the one seen in parallel tests with only mechanical stress applied (i.e., planar slip). **Figure 1*b*** shows the formation of anomalous thin-band twins in a Mg alloy induced by a pulsed current in compression tests (11). **Figure 1*c*,*d*** shows dislocation and twin

Downloaded from www.annualreviews.org. Helmholtz Association (ar-410296) IP: 134.94.123.71 On: Mon, 10 Aug 2026 17:14:48

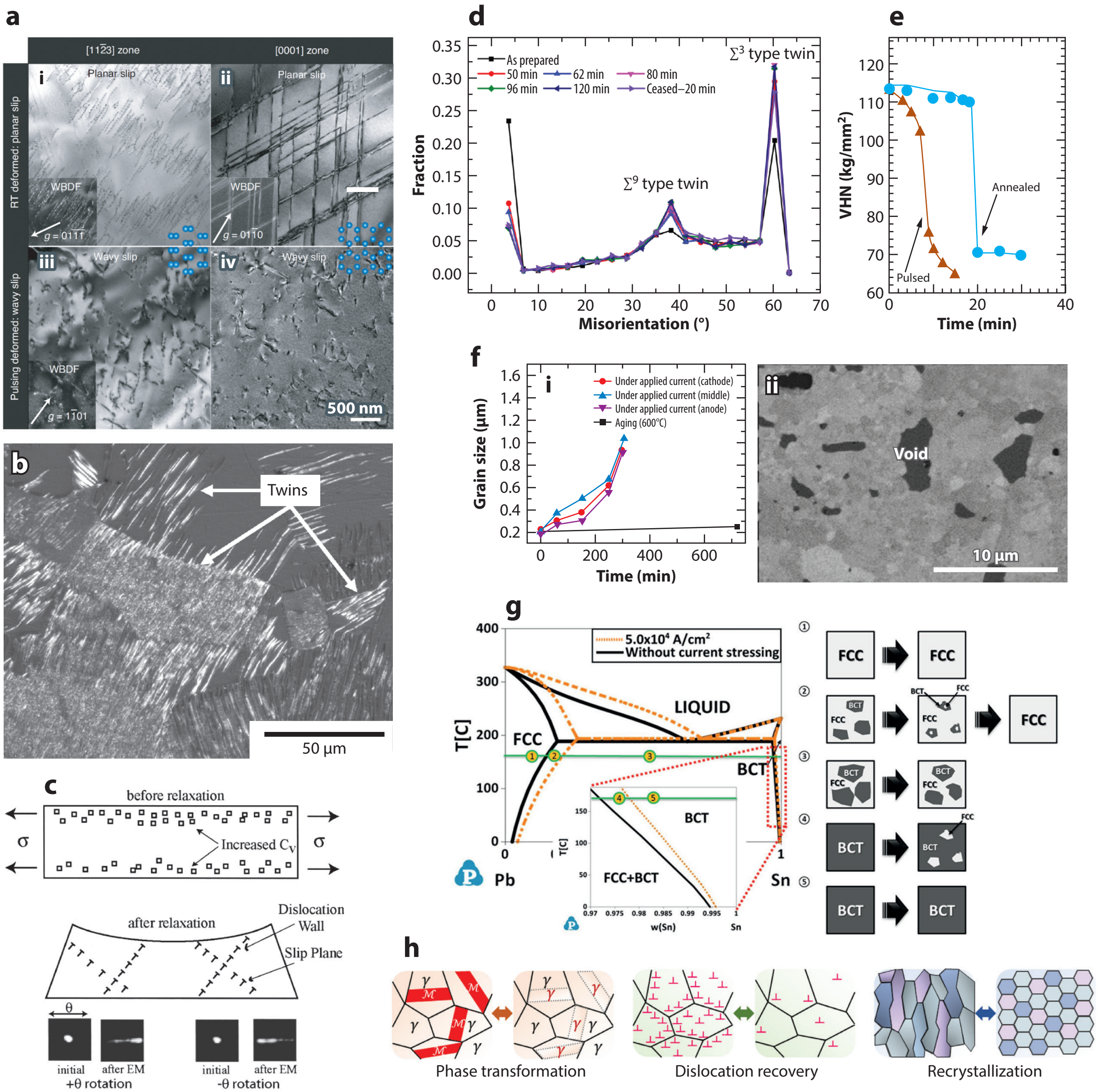

Figure 1

Microstructure and phenomena induced by (*a*, *b*, *e*) the electroplastic effect and (*c*, *d*, *f*, *g*) the electromigration effect. (*a*) Planar slip (*i*, *ii*) and wavy slip (*iii*, *iv*) in Ti-6Al. Panel adapted with permission from Reference 13. (*b*) Anomalous twin formation in a Mg alloy. Panel adapted with permission from Reference 11. (*c*) Dislocation formation in Al. Panel adapted with permission from Reference 12. (*d*) Twin formation in Cu. Panel adapted with permission from Reference 14; copyright 2019 Elsevier. (*e*) Recrystallization temperature decrease in Cu. Panel adapted with permission from Reference 17. (*f*) Anomalous grain growth in Ag–Cu showing (*i*) grain size as a function of time and (*ii*) grain morphology of the anode side after 300 min. Panel adapted with permission from Reference 16; copyright 2019 Acta Materialia. (*g*) Supersaturation effect in Pb–Sn (18) and (*h*) a schematic diagram illustrating electric current–induced phase transformation, dislocation recovery, and recrystallization (21). Panel *g* reproduced with permission from Reference 18 (CC BY-NC-ND 3.0). Abbreviations: BCT, body-centered tetragonal; EM, electromigration; FCC, face-centered cubic; VHN, Vickers hardness number.

formation in pure Al (12) and Cu (14) under a continuous direct current (DC) without external mechanical force. While the results from **Figure 1*a–d*** provide direct evidence of defect formation under electric current, some indirect phenomena also indicate the defect dynamics resulting from interaction with both current and heat. **Figure 1*e*** shows the decrease of recrystallization temperature of cold-worked Cu under a pulsed current (15). **Figure 1*f*** shows the anomalous grain growth (**Figure 1*f*, subpanel *i***) in and microstructure of an Ag–Cu alloy under continuous DC without external mechanical force (**Figure 1*f*, subpanel *ii***) (16). These phenomena suggest that electric current–induced effects in alloys can be divided into two separate processes: electric current–induced defect formation and Joule heating. The former indicates that electric current interrupts lattice ordering and generates defects, such as dislocation density increases, in metals. The latter suggests that Joule heating plays the role of an annealing-like process, elevating system temperature, and induces subsequent recovery, recrystallization, and grain growth to eliminate defects induced by the electric current.

Electric current can also be responsible for the modified phase stability of alloy systems. **Figure 1*g*** shows the supersaturation of Sn in a Pb matrix under electric currents (18). Proposed modeling assumed that an energy term generated by the electric current–induced effective energy was added to the excess Gibbs free energy, as follows:

$$G_{\mathrm{m}}^{\alpha} = {}^{\mathrm{o}}G_{\mathrm{ref.}}^{\propto} + {}^{\mathrm{id}}G_{\mathrm{m}}^{\propto} + {}^{\mathrm{ex}}G_{\mathrm{m}}^{\propto} + {}^{\mathrm{EM-ex}}G_{\mathrm{m}}^{\propto}, \qquad 1.$$

where G_{m}^{α}, ${}^{\mathrm{o}}G_{\mathrm{ref.}}^{\propto}$, ${}^{\mathrm{id}}G_{\mathrm{m}}^{\propto}$, ${}^{\mathrm{ex}}G_{\mathrm{m}}^{\propto}$, and ${}^{\mathrm{EM-ex}}G_{\mathrm{m}}^{\propto}$ are the molar Gibbs free energy, the reference energy of the constituent components, the ideal mixing Gibbs free energy, the excess Gibbs free energy due to nonideal mixing, and the excess Gibbs free energy due to the electromigration effect of the solution phase α, respectively. The simulation agreed well with experimental observation (19). A constitutive model for describing the electric current–induced precipitation hardening effect was also proposed and found in agreement with experimental results (20). These phenomena and models suggest that electric current triggers recovery, recrystallization, and grain growth as well as the phase stability change at elevated environment temperatures to eliminate defects, as shown schematically in **Figure 1*h*** (21).

2.2. Mechanisms

After over fifty years of comprehensive studies, the mechanisms underlying electroplasticity are not yet fully understood. The problem in interpreting the dominant mechanism appears to be due to the presence of many simultaneous effects and the difficulty of distinguishing their contributions. There are multiple challenges to overcome while studying EPE. The physical EPE means that the electron flow has an influence on the physical parameters of the metal and, consequently, on plasticity. In addition to the physical EPE, there is also a technological EPE, which consists of the thermal effect of the high-energy flow of electrons on the material structure, such as by heating the dislocation core (22). The separation of these two effects to determine the magnitude of the physical EPE is the main challenge in developing EPE research methodology. Therefore, the scientific community has attempted a scrupulous, comprehensive description of various mechanisms and factors that can affect the dynamics of changes in the mechanical properties of metal. Despite these efforts, many of the fundamental questions related to the theory of EPE in metallic materials, such as (*a*) the influence of temperature, (*b*) the role of a strong electron flow, (*c*) the role of the magnetic field on dislocation mobility, and (*d*) the synergistic effect of electric and mechanical properties, are still not fully clarified. Thus, the current review presents a view on the fundamental questions of electroplasticity, covering the determination of physical quantities that react sensitively to the effects of current pulses and estimating the magnitude of these changes.

Downloaded from www.annualreviews.org. Helmholtz Association (ar-410296) IP: 134.94.123.71 On: Mon, 10 Aug 2026 17:14:48

Downloaded from www.annualreviews.org. Helmholtz Association (ar-410296) IP: 134.94.123.71 On: Mon, 10 Aug 2026 17:14:48

The first article dealing with the experimental investigation of the impact of electron flow on dislocation mobility was published in 1963 by Troitskii & Likhtman (5) and differed positively from many later works because of the competent physical methodology employed. The work by Kravchenko in 1966 (23) evaluated the threshold current density required for an effective influence on the dislocation mobility. Troitskii (24) published the first investigations related to electric current pulses in the late 1960s. Later, various scientists carried out extensive tests with high current pulses (10^2 to 10^5 A/cm^2, ∼100-μs pulse duration). First, the electric current was shown to weaken atomic bonding due to charge imbalance (25). In parallel, in situ experimental research methods such as electron transmission microscopy (26), digital image correlation (27), and nanoindentation (28) have been used, along with computational methods such as dislocation density–based modeling (29, 30), finite element analysis–based modeling of skin effects (31), and small-scale microstructure-based finite element simulation (32). A recent published review (33) provides a detailed classification of all electroplastic constitutive models under development. At the same time, there is an ongoing attempt to review previously proposed mechanisms from different perspectives to address the issues raised in the literature (29). In recent years, a limited number of new ideas have been proposed, with notable exceptions (25), but instead, previously proposed mechanisms have been more deeply explored. Therefore, the following sections present the different theoretical approaches and investigation methods used for describing EPE.

2.2.1. Electron wind theory and electromigration. Schematically, the force acting on the electrons in the electric field F_{ew} results from the transfer of the conduction electrons to the atoms in the opposite direction (so-called electron wind). The energy generated by the electron wind is very small compared with the energy required for a diffusion step, but it increases in importance when a large number of electrons participate in the process, which is the case at extremely high current densities. Moreover, electromigration theory is generally mentioned when discussing the forces exerted on atoms by an electric field. Electromigration is atomic migration induced by electric currents and is typically considered to be a parallel effect to electroplasticity, since the former highlights migration of individual atoms under an electric field while the latter involves the interaction between dislocations and electric current. To determine the effect of an electric current on dislocation motion, it is therefore useful to consider the forces involved in electromigration. The force induced by an electric field E on individual atoms consists of two components: (*a*) the electrostatic force, f_{es}, which is the direct force of the electric field E on the charged ion, and (*b*) the electron wind force, f_{ew}, which is the momentum exchange of the electrons with the atoms in a collision (9).

The forces that counteract the movement of dislocations can be divided into two categories according to their origin (9): (*a*) the elastic (or chemical) interaction with various structural constraints such as Peierls stress and crystal defects and (*b*) the interaction with elementary excitations of the crystal such as phonons, conduction electrons, and spin waves. The (structural) obstacles can be overcome by thermal motion even at low stresses. In the case of elementary excitations, the dislocations collide with the quasiparticles and exchange energy with them, which slows down the dislocations (9). However, the deceleration force due to collisions is significant only at high dislocation velocities, that is, at velocities greater than 10^{-2} *c* to 10^{-1} *c* (*c* being the speed of sound in the material), where the kinetic energy of the dislocations is greater than the potential energies of structural obstacles. The deceleration force can thus be important for the thermally activated movement of dislocations behind the obstacles (9).

The movement of static dislocations under an electron wind was shown experimentally by Vdovin & Kasumov (34). They studied the transport of dislocations by electrons directly in a

Downloaded from www.annualreviews.org. Helmholtz Association (ar-410296) IP: 134.94.123.71 On: Mon, 10 Aug 2026 17:14:48

high-voltage electron microscope on ultrapure Cu single crystals. The current densities at which dislocation movement could be observed were between 1×10^5 and 1.5×10^5 A/mm^2. The direction of dislocation movement was approximately 30° to the current direction and thus roughly coincided with the <110> direction. Accordingly, a dislocation movement toward the anode took place as predicted by theoretical considerations. According to Vdovin & Kasumov, the velocities of the dislocations were about 1 μm/s. A measurement of the sample resistance showed that the sample did not heat up to more than 100°C. Nabarro (35) examined the dissipated power per unit volume due to the scattering of electrons by a dislocation based on dislocation resistance theorem (9). The first detailed kinetic consideration of the force on dislocations by directed electrons was performed by Kravchenko (23). He hypothesized that a stimulated energy transfer in addition to the perturbation field occurs through the movement of dislocations, provided that the electron drift velocity exceeds the phase velocity. A less rigorous approach to the determination of F_{ew} was proposed by Conrad, who called this electrostatic force, and by Klimov, who called this electron wind force (9, 36). An important part of this calculation relies on the fact that, in addition to the effective electron mass and the average free path length of the electrons, the Fermi velocity is also considered. Fiks (37) carried out a theoretical consideration of the influence of an electric current on the acceleration and deceleration of dislocations. A dislocation moving through the crystal lattice indeed experiences a force equal to the sum of the dragging force and the decelerating force.

2.2.2. Recent advances in understanding the electroplastic effect. Recent publications (27, 29, 38, 39) in combination with previous works (40, 41) have shown that the electron wind effect, perceived as a parameter independent of changes in microstructure (including dislocation, twinning, and orientation at the level of dislocation cells), cannot realistically describe the EPE as previously assumed (42–45). Consider an example to demonstrate this consideration. The stress σ_{ew} acting on the dislocation under the electron wind theory can be expressed by $\sigma_{\text{ew}} = K_{\text{ew}} j/\mathbf{b}$ (j being the electric current density and $\mathbf{b}$ the Burgers vector). In the case of pure aluminum, the theoretical estimate of the coefficient K_{ew} is 7.71×10^{-10} MPa/(A/m^2) (46). **Figure 2** shows σ_{ew} plotted against j. In the range of electric current density frequently reported in research related to electroplasticity (10^6 to 10^9 A/m^2), the estimated value of σ_{ew} is expected to be from 10^{-6} to 10^{-3} MPa. Considering the deformation map of pure aluminum (47), σ_{ew} is significantly lower than the minimum stress at which Coble creep and low-temperature dislocation creep start to activate, at 0.4 T_{m}. This means that beyond the electron wind theory, there must be something else to elucidate the EPE behavior. Molotskii & Fleurov (44) had also shown a four-orders-of-magnitude difference between the experimentally determined value and the theoretical value from electron wind theory. They proposed another model assuming that the dislocation movement is caused by a magnetic field induced by the electric current (44). In addition, indirect effects such as heating of the sample, as well as electric current–induced magnetic fields that cause the pinch effect (9), magnetostrictive effects, and dislocation depinning, have been suggested (44). Sutton & Todorov (48) hypothesized that when the current flows through the metal, the ionic cores of the metal atoms experience a force equal to the Lorentz force on the conduction electrons, which arises from the magnetic field generated by the current, that is, the pinch effect. Molotskii & Fleurov (44) and Molotskii (49) showed that a magnetic field significantly affects dislocation dynamics because it changes the electron spins to their nonequilibrium states, for example, to singlet and triplet states, leading to the dangling bonds forming dislocation cores and obstacles, which then cause the dislocation depinning (44). Nevertheless, the pinch effect and the sample's intrinsic magnetic fields are normally negligible at low current density scenarios (e.g., less than 4–8 × 10^3 A/mm^2) (9). When evaluating experiments, it is important to take these effects into account and, if necessary, to

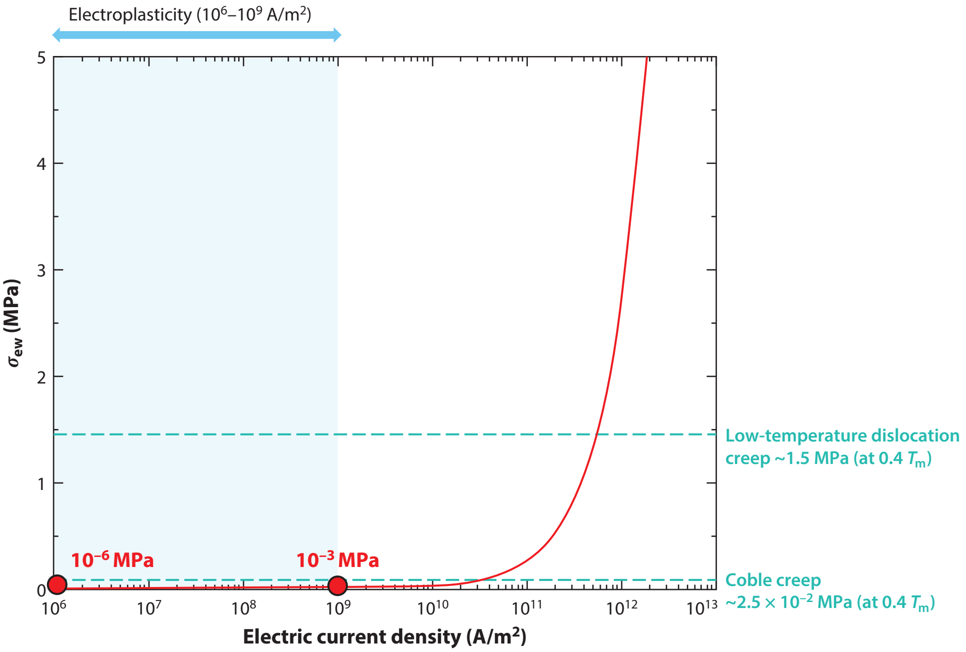

Figure 2

Electron wind stress σ_{ew} as a function of electric current density for pure aluminum.

correct the measurements accordingly. In recent groundbreaking works, evaluation of the extent of the different EPE mechanisms has consistently considered both the heating of samples and the magnitude of the pinch effect during the flow of current (29, 38).

Two complementary techniques are decisive for expanding our knowledge of the EPE. First, the development of electron microscopy techniques to study thin dislocation and twin structures and their structural changes under electric current loading is of particular importance (46). Second, when Conrad and other researchers laid the foundations for evaluating possible EPE mechanisms, they were unable to exceed densities of 8,000 A/mm^2 because of a technical limitation that existed at that time: the capacity of discharge capacitor batteries. Today's level of electrical engineering, which enables the creation of electric double-layer capacitors with a capacitance in the range of several thousand farads (50), allows researchers to approach the predicted threshold current densities when designing pulsed electrical test setups, which will allow the scientific community to evaluate the various EPE mechanisms in a different way (38–43, 50).

2.2.3. The role of mechanical properties on the electroplastic effect. It seems obvious that macroscopically, the occurrence of the electroplastic and electromigration effects of a given material should be correlated with the material's electrical and mechanical properties. For instance, recent work pointed out that electric current–induced twin and hillock formation could be elucidated by using conventional solid mechanics concepts, such as Schmid's law (14). Liu & Lin (51) provide a thorough review of recent work in electroplasticity and electromigration, as well as electrically assisted manufacturing. Although there is no formula yet that directly correlates mechanical properties with electric current effects, the Blech critical product from electromigration theory may provide a hint (52). The Blech critical product is formulated as $jL = \frac{\sigma\Omega}{epz^*}$, where j is the current density, L is the sample strip length, σ is the back stress, Ω is the atomic volume of the

Downloaded from www.annualreviews.org. Helmholtz Association (ar-410296) IP: 134.94.123.71 On: Mon, 10 Aug 2026 17:14:48

Downloaded from www.annualreviews.org. Helmholtz Association (ar-410296) IP: 134.94.123.71 On: Mon, 10 Aug 2026 17:14:48

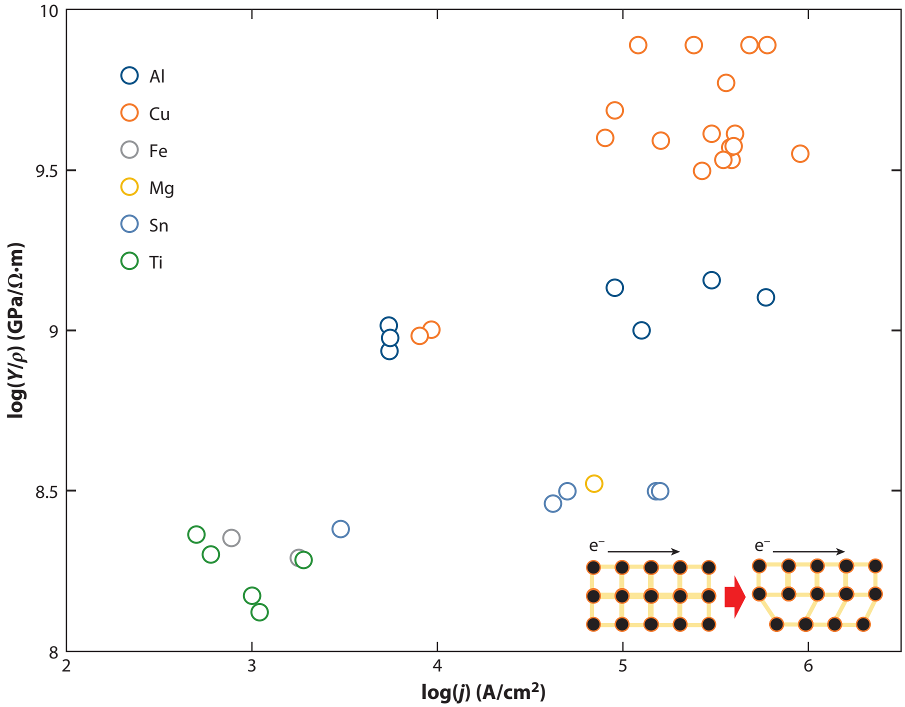

Figure 3

Plot of log(Y/ρ) versus log(current density) for common alloy systems under an electric current. Data for Al from References 52 and 54–57. Data for Cu from References 14, 17, and 58–63. Data for Fe from Reference 57. Data for Mg from Reference 11. Data for Sn from References 64–66. Data for Ti from References 13, 57, 67, and 68.

material, ρ is the resistivity, e is the fundamental electron, and z^* is the effective charge. Tu (53) suggested that the back stress could be approximated by using Young's modulus multiplied by the elastic limit (i.e., $\sigma = Y\Delta\epsilon$). In this way, he successfully elucidated why critical current density for a eutectic SnPb solder is two orders of magnitude smaller than that for Al and Cu. Hence, it seems particularly relevant to correlate the electroplastic or electromigration effect with the Young's modulus Y and resistivity ρ_R.

Figure 3 plots the Y/ρ_R ratio and current density j with logarithmic scales for various material systems where the electroplastic or electromigration effect was observed (11, 13, 17, 52, 54–68). It should be noted that the exact critical value of current density for which electric current–induced deformation initiates was very difficult to obtain. That is why the current densities shown in **Figure 3** are the nominal values reported in the literature when the phenomena induced by the electric currents take place; that is, the reported current densities may be equal to or larger than a material's specific critical values. A proportional relationship between the Y/ρ_R ratio and the current density was found. This suggests that materials with high electric conductance and a high elastic constant would have high resistance against electric current–induced deformation, in terms of either the electroplastic or electromigration effect.

This can be understood by the fact that at a given current density, the materials with high conductance are likely to be subject to low electron wind forces, and the materials with high elastic constant are less likely to be plastically deformed. As a result, the critical current densities for Cu and Al would be in the range of 10^5–10^6 A/cm^2, while those for Ti or Sn would be only

10^2–10^3 A/cm^2. The electrical properties influence the EPE, but the mechanical properties also play an important role. This understanding opens the door for alloy design (as in electronic interconnectors in microelectronic applications, which need to withstand very high current densities) as well as for process design for electric current–assisted manufacturing.

3. PLASTICITY OF CERAMICS UNDER AN ELECTRIC FIELD

Ceramic materials are not known to be particularly ductile. Most ceramics are brittle at low and medium temperatures because the large critical resolved shear stress decreases from a few gigapascals to some tens of megapascals only at high temperatures (69). This introduces a high creep resistance at low and medium temperatures ($T < 0.4\ T_{\mathrm{m}}$), which is desirable for many ceramics applications as it limits their processibility during manufacturing and the break-away strains at operating conditions. Electroplasticity offers a way to enhance the ductility during manufacturing at lower temperatures. Sintering under considerable electric fields and currents can also introduce a remnant enhancement toward ductility at room temperature. Most reports were on polycrystalline ceramics (in particular on high-strain superplastic deformation, where the uniform elongation exceeds 100%), but single crystals were also affected by electric fields.

The main mechanisms for creep and plastic deformation in polycrystalline ceramics are grain boundary sliding (GBS), which also accompanies Nabarro–Herring and Coble creep (70), and dislocation glide. GBS was found to be the main mechanism for field-enhanced deformation in polycrystals (70). A modification of the grain boundaries induced by applied electric fields should therefore change the creep behavior of ceramics. It became evident that whereas superplasticity (elongation > 100%) requires nanosized grains during field-less deformation (21, 71), it can take place in polycrystals with micron-sized grains when assisted by electric fields because the space charge layers involved in GBS are affected by the field.

True metal-like plastic behavior would require the presence of many dislocations in the ceramics (72). A few materials (such as strontium titanate) present an inverse brittle-to-ductile transition and can deform at room temperature (69). If a suitable dislocation density can be introduced by electric field treatment, a range of new opportunities opens. Conventional sintering, the standard densification method for ceramics, yields ceramics with a low density of dislocations and dislocation sources. In other words, the brittleness of ceramics may be interpreted as being due to their inherent lack of dislocation coupled with the established conventional production method. Electric power, however, can introduce dislocations in ceramics.

How electric fields can modify the plastic and superplastic behaviors of ceramics is presented in the next sections. As mentioned above, we can categorize two types of electric field–assisted plasticity: in situ and ex situ (or remnant). Then, in Section 3.2, we investigate the potential mechanism behind the observed field-enhanced effects.

3.1. Electroplastic Behavior

Electroplastic mechanical behavior is observed during the application of the field (in situ), but also after the field is switched off (ex situ). Electric field–assisted creep measurements show amplified strain rates with reduced corresponding flow stresses. The materials even behave superplastically with very high strain to failure. The mechanical properties are modified even after the field is switched off (ex situ): Young's modulus, hardness, creep rates, and fracture strains were found to be significantly affected, indicating ductility.

3.1.1. In situ. The interaction of an electric current or field with ceramics involves both thermal and athermal effects. The thermal effect, which is Joule heating due to the ohmic voltage loss, is

Downloaded from www.annualreviews.org. Helmholtz Association (ar-410296) IP: 134.94.123.71 On: Mon, 10 Aug 2026 17:14:48

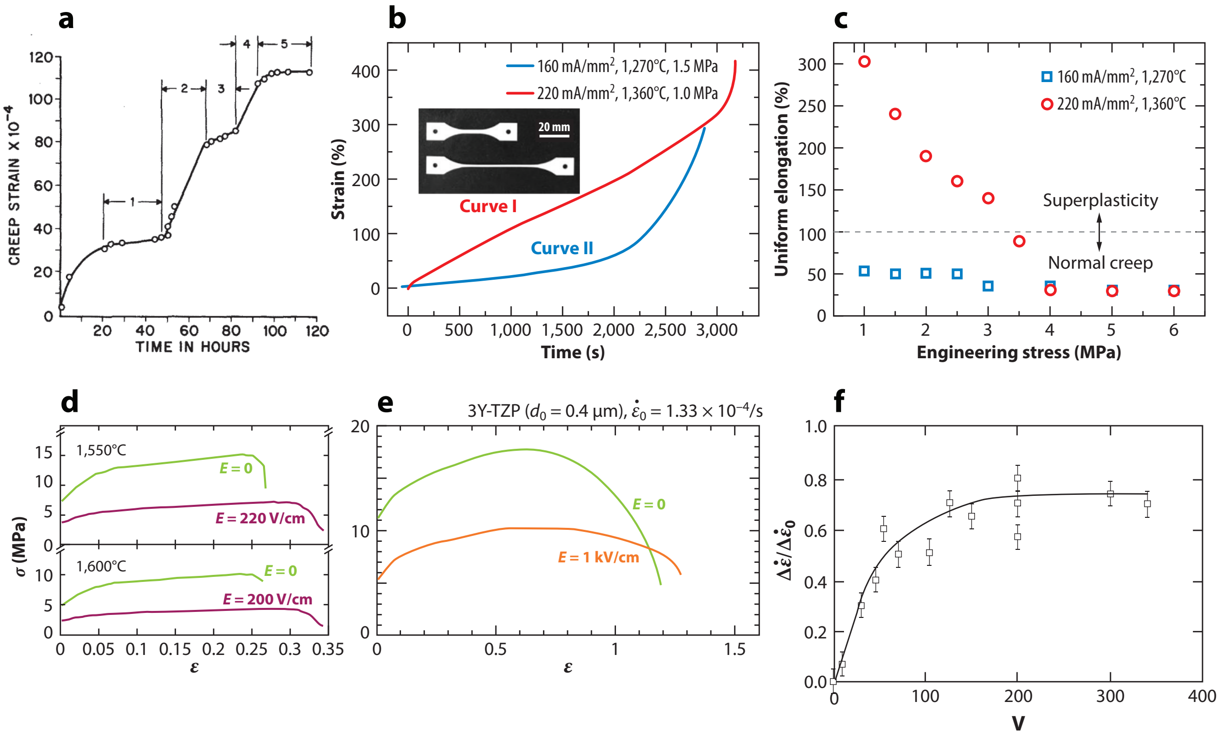

Figure 4

Electric field–assisted creep deformation behavior of various ceramic materials. (*a*) Creep strain of a MgO single crystal under an electric field at 1,000°C. Segments 1, 3, and 5 show the creep rate without an electric field, whereas segments 2 and 4 show the creep rate with the electric field switched on. (*b*) Creep deformation of zirconia at different current densities. The inset shows the elongation of the specimen without and with the applied electric field. (*c*) Creep and superplasticity regime demarcation based on current densities (74). (*d*) Stress–strain curves of polycrystalline MgO under 220 V/cm at 1,550°C and 1,600°C (78). (*e*) Stress–strain curves for 3 mol% yttria-stabilized ZrO_2 (3Y-TZP) ceramics with and without an electric field (79). (*f*) Strain rate dependency with an electric field for ice (80). Panel *a* reproduced with permission from Reference 73; copyright 2004 AIP Publishing. Panels *b* and *c* adapted with permission from Reference 74; copyright 2022 Acta Materialia. Panel *d* adapted with permission from Reference 78; copyright 2000 Acta Metallurgica. Panel *e* adapted with permission from Reference 79; copyright 2008 Springer Science. Panel *f* adapted with permission from Reference 80.

considered in the research by, for example, lowering the furnace temperature to compensate for the sample heating or in interpreting the data. Therefore, our focus is on the athermal effect, which is sometimes called the direct field effect.

First, Neiman & Rothwell (73) showed the effect of 500 V DC (in this pioneering work of 1963, only voltage without the sample dimension was reported) on the creep behavior of single-crystal MgO at 1,000°C during a three-point bending test. **Figure 4*a*** shows the creep strain as a function of time with and without the application of an electric field. The creep rate reverted to its original value after switching off the electric field. The largest creep rate reached was 5.8 × 10 s^{-8}. The increase in creep rate was unlikely to be due to Joule heating, as the electrical power input remained below 1 W. This case highlights that electroplasticity in ceramics is not contributed only by grain boundaries. The field-affected movement of charged dislocations is also responsible.

To continue with a very impressive example of how electric fields can enhance deformation, we look at the work of Liu et al. (74), who studied the tensile creep behavior of a 3 mol% yttria-stabilized ZrO_2 polycrystalline (3Y-TZP) ceramic under a DC electric field inducing

Downloaded from www.annualreviews.org. Helmholtz Association (ar-410296) IP: 134.94.123.71 On: Mon, 10 Aug 2026 17:14:48

flash-sintering conditions. During flash sintering, the sample densifies under strong electric fields and rather low furnace temperatures within seconds while a rapid increase of conductivity and large current flows are observed (75). An accelerated self-diffusion, the generation of atomic defects and enhanced mass-transport phenomena that takes place at higher temperatures, is expected during the flash event (76, 77). **Figure 4*b*** shows the tensile elongation of 3Y-TZP under two different current densities, 160 and 220 mA/mm^2, sample temperatures of 1,270°C and 1,360°C, and a constant load of 1.5 and 1.0 MPa. A higher current density results in a higher creep rate, as expected. In addition, a higher current density (200 mA/mm^2) also results in very large uniform elongation (up to 300%) (**Figure 4*c***), causing the material to behave as a superplastic.

Conrad (1) and Conrad & Yang (78) showed that the flow stress of polycrystalline MgO reduced by half with the application of an electric field of 220 V/cm (**Figure 4*d***). When the electric field was intermittently switched on and off, the flow stress was reversibly changed. A similar trend was observed for 3Y-TZP ceramics as well (**Figure 4*e***) (79). Here, a very high field of 1 kV/cm was applied across dog-bone shaped samples at a furnace temperature of 1,500°C. The specimen under the field was elongated considerably more than the specimen without the field. An unconventional case of electroplasticity is also illustrated, as ice might be categorized as a ceramic in certain aspects. Petrenko & Schulson (80), with the help of a complicated setup, demonstrated that the application of an electric field across ice enhances plastic deformation. **Figure 4*f*** shows the change in strain rate with the applied voltage.

Yoshida & Sasaki (76) induced superplasticity in 3Y-TZP by using a DC field (120 V/cm) at a lower furnace temperature of 1,000°C as compared with Yang & Conrad (79). At a strain rate of 0.001 s^{-1}, a strain of nearly 135% was achieved in the case of the ceramic subjected to an electric field, whereas the sample without an electric field underwent a brittle fracture (**Figure 5*a***). Motomura et al. (81) experimentally demonstrated the athermal effect of an electric field on the plastic deformation of 3Y-TZP. The ceramic was subjected to three-point flexural loading under the flashed state with a current density of 67 mA/mm^2. **Figure 5*b*** shows the flow stress as a function of the strain with and without an electric field. Without the field, the zirconia beam suffered brittle fracture, whereas with the field, the sample could be bent to a large extent without failure. The sample temperature was measured to be 1,230°C, and it would not have been possible to bend zirconia without an electric field (by using only thermal energy and keeping the furnace at 1,230°C). This is clear evidence of an athermal effect of the electric field and that the plasticity cannot be explained by the elevated temperature resulting from Joule heating alone (81). In the pursuit of separating the thermal and athermal effects, very low electric fields were applied by Cao et al. (82, 84) to understand the change in viscosity of porous ceria ceramics. The behavior was proven to be symmetric in tension and compression, both with and without an electric field. A clear decrease in uniaxial as well as bulk and shear viscosities was already measured for alternating current (AC) fields below 30 V/cm (**Figure 5*c***) (84). By implementing an artificial temperature rise into a phenomenological model of viscosity, it was possible to reproduce the athermal field effect. This approach enables the quantification of the effect of electric fields in terms of the equivalent thermal energy transferred to the sample but does not give any hint about the real nature of the phenomena (10).

As mentioned above, the key to observing superplasticity is to maintain a constant grain size and prevent grain growth during deformation. An optimum current density was found for obtaining the highest strain. A further increase in current density results in grain growth, which in turn restricts the GBS, thereby increasing the flow stress (**Figure 5*d***) (85).

To finish, electroplasticity has also been observed in nonoxide ceramics. Shen et al. (86) conducted deformation experiments on dense α- and β-SiAlON ceramics using a field-assisted sintering technique and spark plasma sintering (FAST/SPS) furnace with a hot press for

Downloaded from www.annualreviews.org. Helmholtz Association (ar-410296) IP: 134.94.123.71 On: Mon, 10 Aug 2026 17:14:48

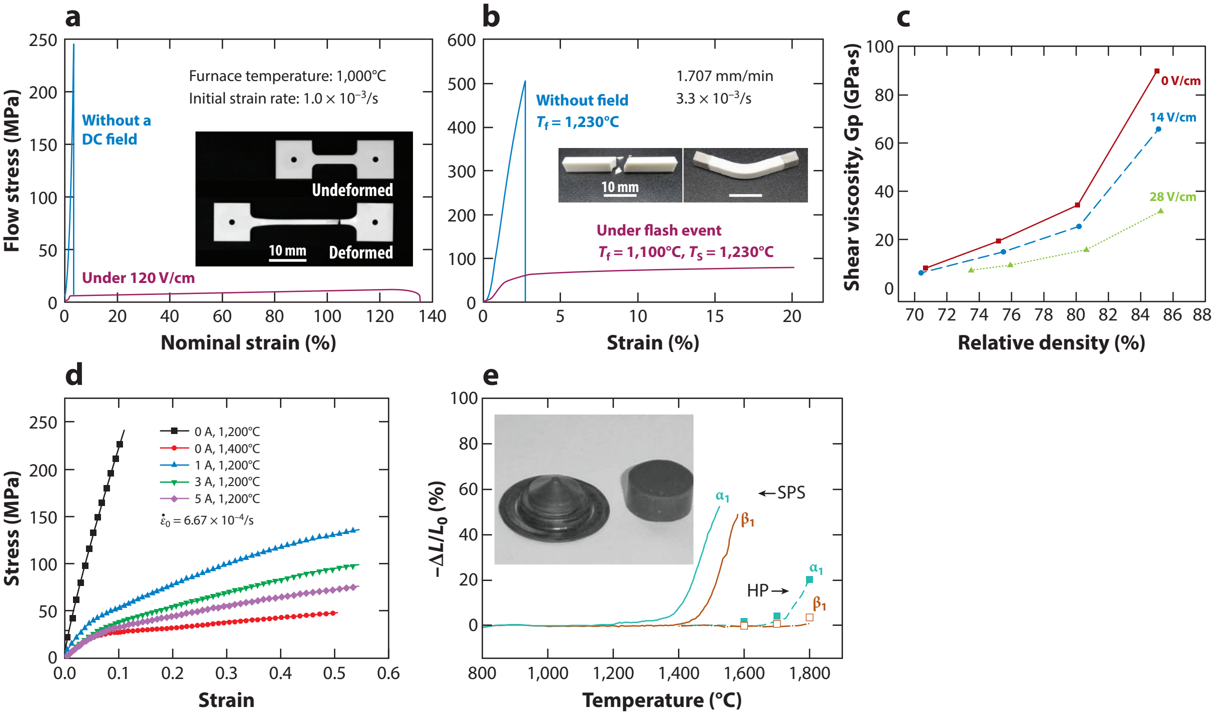

Figure 5

Electric field–assisted superplasticity of oxide and nonoxide ceramics. (*a*) Stress–strain curve of dense 3Y-TZP deformed in tensile mode without and with a DC field of 120 V/cm. Panel adapted with permission from Reference 76; copyright 2017 Acta Materialia. (*b*) Stress–strain curve of dense 3Y-TZP deformed in bending mode with and without a current density of 67 mA/mm^2. The inset shows the brittle fracture and complete bending of the zirconia beam. Panel reproduced with permission from Reference 81; copyright 2022 The Author(s) (CC BY-NC-ND 4.0). (*c*) Change in shear viscosity induced by AC fields for yttria-doped ceria measured at a constant sample temperature. Panel adapted with permission from Reference 84. (*d*) Stress–strain behavior of 3Y-TZP with an electric field in an oxygen-lean atmosphere. Panel adapted with permission from Reference 85. (*e*) Strain–temperature relation of SiAlON ceramics being deformed with (SPS) and without (HP) an electric field. The inset shows the deformed SiAlON ceramic specimen. Panel adapted with permission from Reference 86; copyright 2003 Wiley-VCH GmbH. Abbreviations: AC, alternating current; DC, direct current; HP, hot pressing; SPS, spark plasma sintering; 3Y-TZP, 3 mol% yttria-stabilized ZrO_2 polycrystalline.

comparison. FAST/SPS is an electric current–assisted consolidation technique and was also used for current-assisted deformation. **Figure 5*e*** shows the strain versus the temperature, where the deformation in SPS takes place at a much lower temperature (1,400–1,500°C) as compared with hot pressing (1,700–1,800°C).

3.1.2. Ex situ. Electric field treatment of ceramic materials at a high temperature can induce remnant effects and enable plasticity afterward at a low temperature. The difficulty may be in retaining the possible out-of-equilibrium state in the material and making use of it during the deformation test. Indentation measurements are useful to test the local mechanical properties and indirectly assess any change in the plasticity of the indented material.

Masuda et al. (83) evaluated the micromechanical response of fully stabilized zirconia, which was exposed under an AC electric field of 220 V/cm and a current density of 400 mA/mm^2 (hereafter referred to as "flashed"). To avoid the recovery of the defects, the group quenched the flashed zirconia samples for characterization, which may provide information close to that of an in situ study. **Figure 6*a*,*b*** shows the contact modulus (*E*) and hardness (*H*) of flashed and nonflashed

Downloaded from www.annualreviews.org. Helmholtz Association (ar-410296) IP: 134.94.123.71 On: Mon, 10 Aug 2026 17:14:48

Downloaded from www.annualreviews.org. Helmholtz Association (ar-410296) IP: 134.94.123.71 On: Mon, 10 Aug 2026 17:14:48

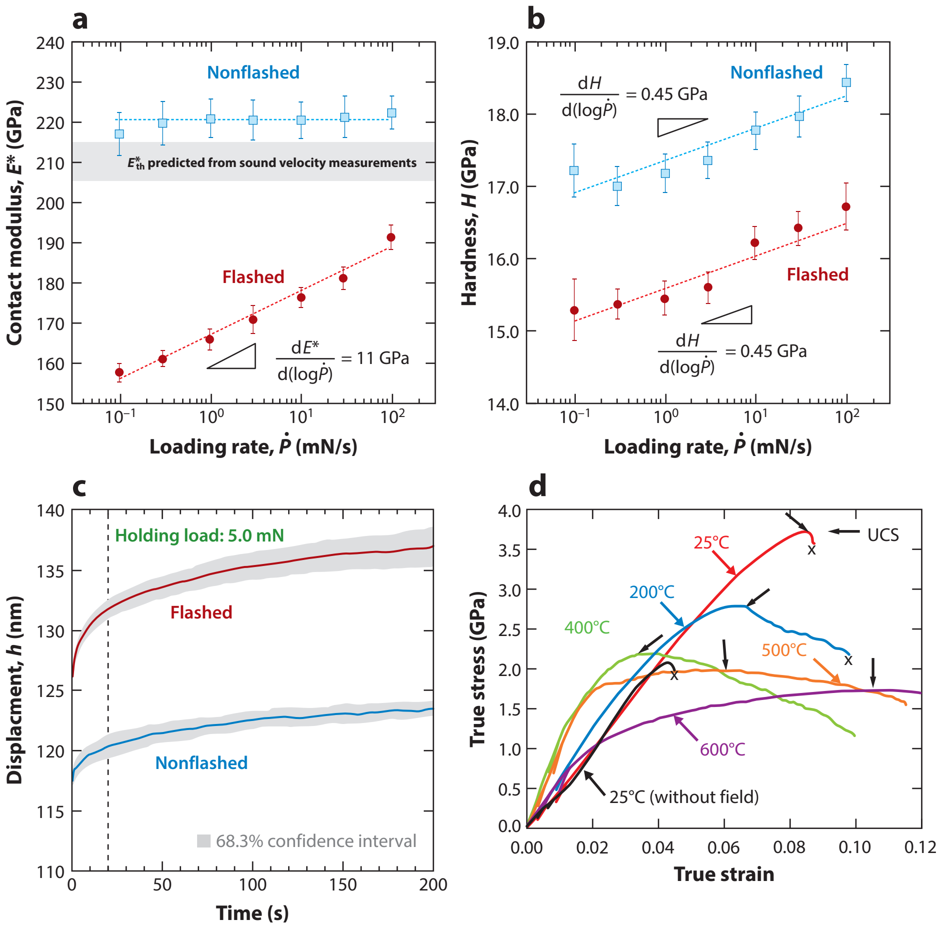

Figure 6

Ex situ effect of an electric field on the mechanical behavior of zirconia ceramics. (*a*) Contact (indentation) modulus as a function of loading rate showing constant elastic behavior for the nonflashed samples and rate-dependent behavior for flashed samples, interpreted as anelastic (viscoelastic) deformation. (*b*) Hardness with respect to loading rates based on nanoindentation experiments on flashed and conventionally sintered zirconia. (*c*) Creep curves obtained from nanoindentation for flashed and conventionally sintered samples. (*d*) Stress–strain curves obtained from compression of micropillars at different temperatures. Panels *a–c* adapted from Reference 83 (CC BY 4.0). Panel *d* adapted from Reference 87 (CC BY 4.0). Abbreviation: UCS, ultimate compressive stress.

zirconias as a function of the loading rate. The H values of the flashed samples were 1.8 GPa lower than the ones of the nonflashed samples, independent of the loading rate. The lower values in flashed samples were attributed to recoverable anelastic (viscoelastic) strain.

A nanoindentation creep experiment on flashed and nonflashed samples (**Figure 6*c***) revealed that the initial displacement in the primary creep regime was higher for the flashed sample, whereas the creep rate was similar for both flashed and nonflashed samples in the steady-state creep regime. Such a behavior is attributed to time-dependent anelastic deformation, possible mechanisms for which are presented in the next section (83).

In addition, uniaxial microcompression tests of pillars in an instrumented scanning electron microscope give complementary information on the deformation behavior of a representative

Downloaded from www.annualreviews.org. Helmholtz Association (ar-410296) IP: 134.94.123.71 On: Mon, 10 Aug 2026 17:14:48

volume element. By using a heating stage, the investigations can be carried out as a function of temperature (87). As shown in **Figure 6*d***, yttrium-stabilized zirconia (YSZ) micropillars at room temperature sustain large strain (∼8%) compared with their bulk counterpart (∼2%) due to stress-induced martensitic transformation toughening. However, the pillars fracture catastrophically after the nucleation of cracks. In comparison, a brittle-to-ductile transition of the fracture mode is observed at 400°C in flash-sintered YSZ, much lower than the ∼800°C reported for conventional bulk YSZ. The enhanced plasticity at elevated temperatures arises from the transition from phase transformation toughening to dislocation creep.

3.2. Mechanisms

The applied electric field heats up the sample due to Joule heating. The rise in temperature may be attributed to the enhanced creep rates and changes in mechanical responses. However, the mechanical response of the ceramic at an equivalent temperature without any applied electric field is rather brittle. The creep activation energy was lowered and the stress exponent changed in some cases. The presence of photoluminescence in flashed samples indicated that point defects were created by the electric field. Furthermore, the grain boundaries were transformed (amorphized) and arrays of dislocations appeared in the material.

3.2.1. Joule heating. The rate of creep $\dot{\varepsilon}$ depends on a few parameters such as the material itself, grain size d, flow stress σ, and temperature T:

$$\dot{\varepsilon} = A\sigma^n d^{-p} \exp(-Q/RT), \tag{2}$$

where A is a material constant, n the stress exponent, p the grain size exponent, Q the activation energy, and R the molar gas constant. The achievable creep deformation is also a function of those parameters. It is therefore natural to first propose Joule heating as the main possible cause for enhanced creep deformation when current flow is present. Using the equation given above, the creep data obtained by Owen & Chokshi (88) without an electric field were extrapolated to the same sample temperature of the experiments under electric loading by Yoshida & Sasaki (76). The strain rate obtained by Yoshida & Sasaki with an electric field was nearly one order of magnitude higher than the extrapolated data (**Figure 7*a***), which excludes Joule heating from being the only reason for the enhanced creep observed.

For electric field–assisted bending experiments on YSZ ceramics, Motohashi et al. (91) showed that the flow stress of ceramics under an electric field is higher even though Joule heating is taken into consideration. For example, a furnace temperature of 1,100°C and sample temperature of 1,230°C yield a similar flow stress as observed at 1,450°C without an electric field (**Figure 7*b***). As creep rates do not match by extrapolation to the sample temperature, additional factors must be responsible for the observed behavior.

3.2.2. Change in stress exponent and activation energy. The determination of the stress exponent n in the empirical stress–strain rate relationship (Equation 2) is an important way to identify the rate-controlling mechanism, as it is also for the case of electroplastic deformation.

For zirconia, Liu et al. (74) observed the following change in the values of n for different current densities and mechanical loadings: $n \approx 1$ for a current density of 160 mA/mm^2, indicating that the creep is dominated by a diffusion-controlled process (e.g., Nabarro–Herring or Cobble creep); $n \approx 2$ for a current density of 220 mA/mm^2 and $\sigma \leq 3.5$ MPa, interpreted as dislocation-flow accommodated GBS; and $n \approx 3$ for the same current density but with $\sigma > 4$ MPa, understood as dislocation flow.

On the other hand, for cubic zirconia at 1,000°C and under 30 V/cm (**Figure 7*c***), the stress exponent was not affected, suggesting that the electric field did not change the rate-controlling

Downloaded from www.annualreviews.org. Helmholtz Association (ar-410296) IP: 134.94.123.71 On: Mon, 10 Aug 2026 17:14:48

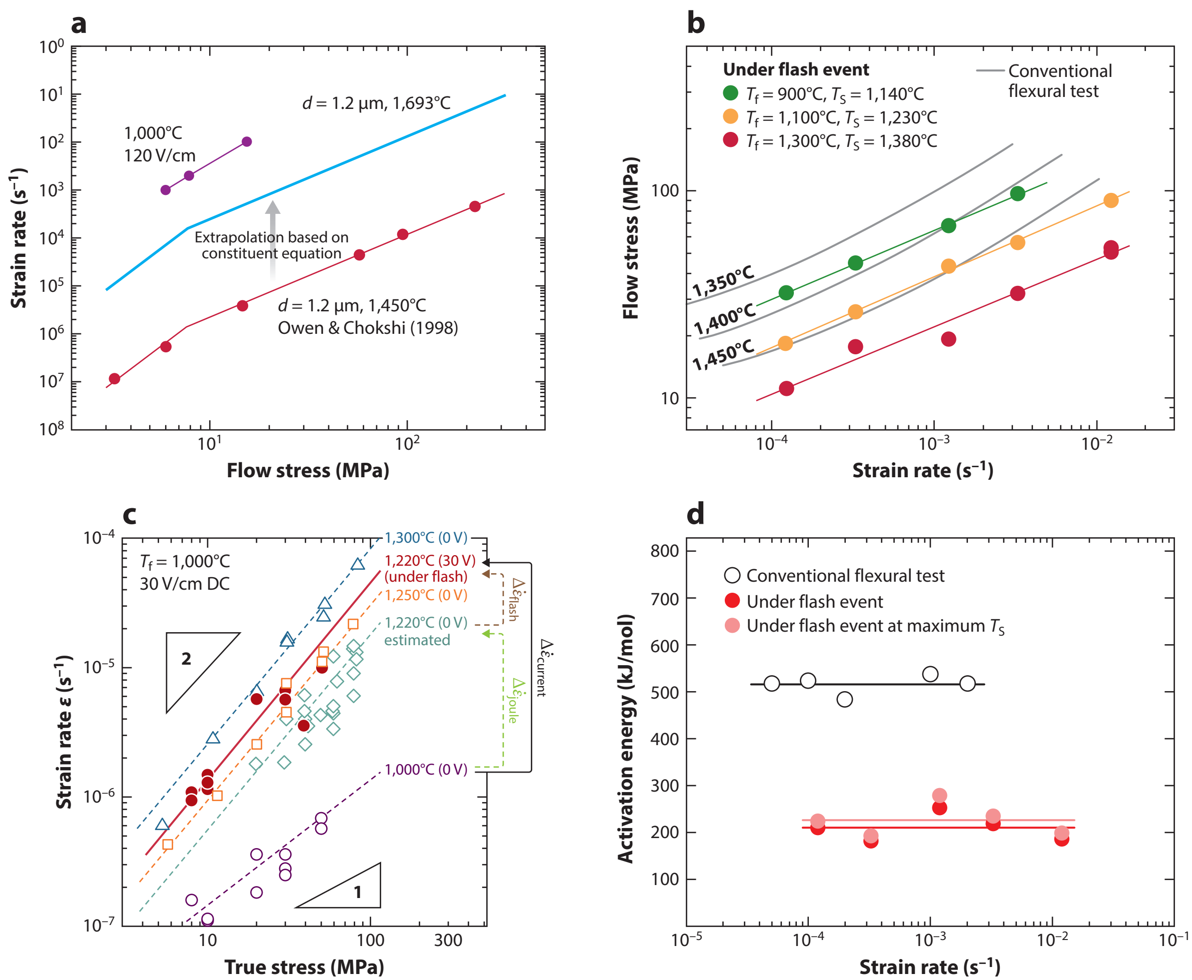

Figure 7

Post-analysis of deformation behavior for identifying the contribution of an electric field. (*a*) Strain rate versus flow stress for tetragonal zirconia (3Y-TZP) deformed at 1,000°C under 120 V/cm. (*b*) Flow stress versus strain rate for flexural testing of 3Y-TZP ceramics under an electric field (flash) in comparison with conventional tests (without field) from Reference 91. (*c*) Strain rate versus true stress of cubic zirconia at 1,000°C under 30 V/cm (89). Estimated values for 1,220°C (0 V) are from Reference 90. (*d*) Activation energy of conventional and flashed flexural testing of 3Y-TZP ceramics (81). The conventional flexural test results are from Reference 91. Panel *a* adapted with permission from Reference 76; copyright 2017 Acta Materialia. Panels *b* and *d* adapted with permission from Reference 81; copyright 2022 The Author(s) (CC BY-NC-ND 4.0). Panel *c* adapted with permission from Reference 89; copyright 2022 Elsevier.

deformation mechanism (74, 92, 93). The stress exponent for gadolinia-doped ceria also did not change from its fieldless value of 2 when subjected to fields of 7–20 V/cm AC (50 Hz) and current densities of 25 mA/mm² and 200 mA/mm², although the strain rate doubled for the smaller current density and was amplified by a factor of 70 for the higher current density compared with fieldless creep (94). The deformation mechanism was stated as GBS both with and without AC or DC current. However, different materials, substitutions, and a small number of impurities at the grain boundaries can completely change the deformation mechanism(s).

As shown in **Figure 7*d***, the activation energy for the high-temperature plastic flow of TZP was calculated by plotting flow stress against the inverse of the sample temperature. A lower activation energy of 210 kJ/mol was calculated for the plastic deformation, which is significantly lower than the typical activation energies of oxide ceramics (500–600 kJ/mol). The lowering of the activation energy was interpreted as a lower energy being required for Zr cation diffusion. The formation of oxygen vacancies from electrochemical reduction might enhance the cation diffusion, thereby accelerating the rate of deformation (74, 81, 89).

3.2.3. Modified distribution of point defects. The application of an electric field may result in a different type and concentration of (mobile) defects, induced only thermally. For example, the formation of extrinsic oxygen vacancies, which may modify the behavior of cation defects and lead to a higher grain boundary mobility, has been observed in zirconia (95–97). To investigate the defect chemistry of zirconia influenced by the electric field, Yamashita et al. (98) characterized the photoluminescence (PL) of conventionally sintered, conventionally flashed, and isothermally flashed samples (**Figure 8*a***). The sintered samples were illuminated with white and UV light

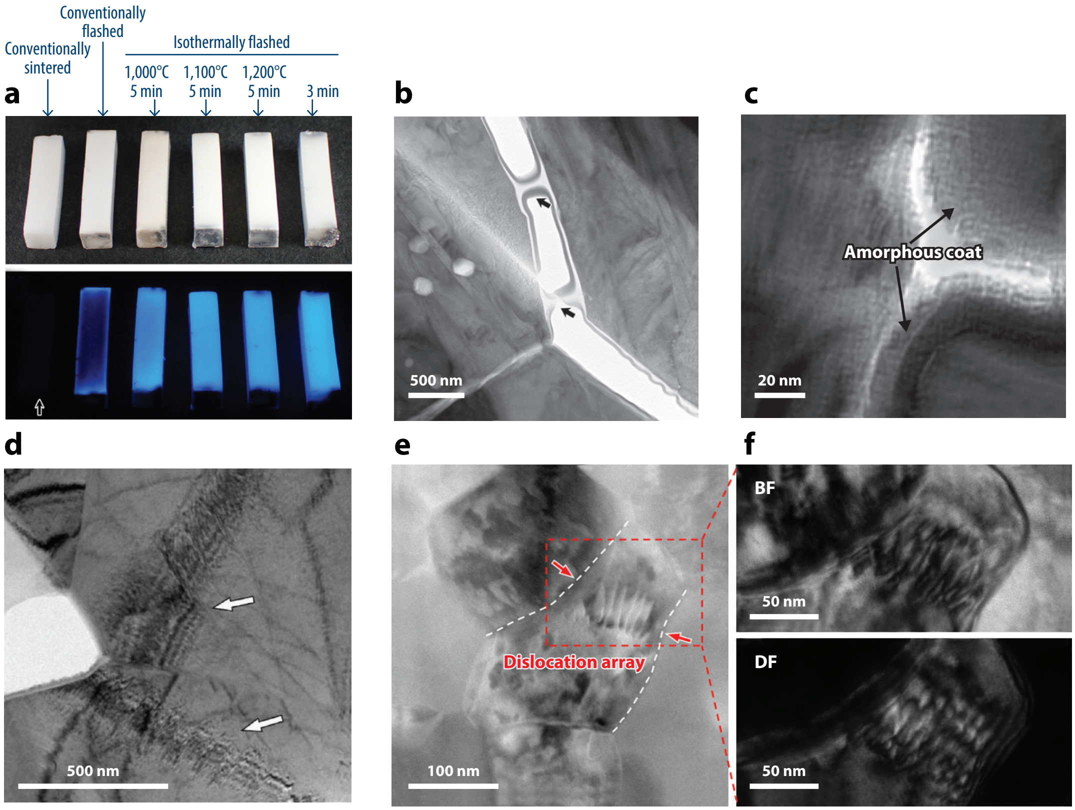

Figure 8

Microstructural evidence for mechanisms leading to electroplasticity in ceramics. (*a*) Photoluminescence of conventionally sintered, conventionally flashed, and isothermally flashed 3 mol% yttria-stabilized tetragonal zirconia polycrystalline (3Y-TZP) ceramics under a 365-nm UV light. Panel adapted with permission from Reference 98; copyright 2020 Elsevier. (*b*) Transmission electron micrograph (TEM) of a grain boundary showing amorphous film in monoclinic zirconia. Panel adapted with permission from Reference 101; copyright 2018 American Ceramic Society. (*c*) Amorphous grain boundary in SiAlON after electric field processing. Panel adapted from Reference 102 (CC BY 4.0). (*d*) TEM of deformed zirconia under 220 mA/mm^2. Panel adapted with permission from Reference 74. (*e*) TEM of flash-sintered 3Y-TZP showing the presence a dislocation arrays, which are not observed in conventionally sintered material (87). (*f*) The array of the boxed region in panel *e* with more detail in bright field (BF) and dark field (DF). Panels *e* and *f* adapted from Reference 87 (CC BY 4.0).

Downloaded from www.annualreviews.org. Helmholtz Association (ar-410296) IP: 134.94.123.71 On: Mon, 10 Aug 2026 17:14:48

(365 nm). The flashed samples emitted blue PL, suggesting the presence of singly ionized associated oxygen vacancy defects (AODs). Furthermore, detailed analysis of the PL spectra confirmed that the increased PL intensity was due to the high concentration of AODs introduced by the flash phenomenon (99). The intensity of PL was lower in the case of conventionally flashed samples because the furnace temperature was lower, and the reaction leading to the formation of defects took place only on the surface. In the case of isothermal flash, the point defects were formed in the bulk of the sample and not just at the surface. It is noteworthy that PL persisted even after a high-temperature annealing of the flashed samples. Such remnant effect has also been observed for zinc oxide (100), where contacting and noncontacting fields induced change in the defect population as evidenced by the ratio of near-band-edge to deep-level-emission signals. It is reasonable to think that the point defects induced by the electric loading at a high temperature are related to the anelastic behavior described above.

3.2.4. Grain boundary alterations. A probable explanation for enhanced GBS and reduction in flow stress under an electric field may be that the space charge layers at the grain boundaries are modified under electric loading (and remain after removal of the field). In a response to lattice stress and broken bonds, the grain boundary restructures by segregating point defects to the grain boundary core. The charge brought by these defects at the grain boundary plane is shielded by an accumulation of point defects with inverse polarity next to the grain boundary core. As the space charge layer has its own internal electric field, it is highly probable that the application of a macroscopic electric field affects the space charge layer structure and dopant segregation (103). As newly shown for strontium titanate (STO), static electric fields applied parallel and perpendicular to the grain growth direction affect the grain boundary structure (103, 104). The thickness of the grain boundary is modified under electric loading (for example, from 0.80 nm on the positive side to 0.36 nm at the negative electrode under 50 V/mm) and can even lead to its decomposition (103). The creation of oxygen vacancies in STO samples is proven by X-ray photoelectron spectroscopy showing the presence of Ti^{3+} and Ti^{2+}. These positively charged oxygen vacancies are very mobile in comparison with cations and create a gradient under static electric field conditions. Accordingly, the oxide becomes reduced (oxidized) at the negative (positive) electrode. This significantly changes the grain boundary mobility, grain growth, and resulting creep deformation within the sample. In addition, if grain boundary dislocations can act as both source and sink for vacancies, the application of an external electric field influences the vacancy flux across dislocations. While STO is the only example where the effect of electric fields on grain boundary mobility is well understood and modeled in detail, other materials such as barium titanate seem to behave similarly. In contrast, the grain growth in magnesium aluminum spinel and rare-earth doped ceria does not seem to change under electric fields (82, 105).

A more unexplored grain boundary phenomenon is amorphization in the presence of an electric field (106). Morisaki et al. (101) made it possible to sinter monoclinic zirconia with the aid of a DC electric field, overcoming the usual shattering of zirconia due to the large volume expansion from the tetragonal to monoclinic phase. This was facilitated by grain boundary amorphization, which was observed to be due to the severe reducing condition arising from the electric current–induced flashed state (**Figure 8*b***). It has been demonstrated by Yoshimura et al. (107) and Hayakawa et al. (108) that it is almost impossible to amorphize zirconia by quenching from the melting temperature. These results point toward the possibility of a transient amorphous film in the grain boundary that is formed due to the combination of both electric current and applied stress (101, 109). Yet other evidence for grain boundary structure modification with an applied electric field was shown by Morita et al. (110). Rapid crack healing in the case of cubic zirconia was observed after flashing. The flashed healing rate was twice that of static healing without an electric field at 1,230°C.

Downloaded from www.annualreviews.org. Helmholtz Association (ar-410296) IP: 134.94.123.71 On: Mon, 10 Aug 2026 17:14:48

The enhanced diffusion caused the cracks induced by indentation to heal. Nonoxide ceramics are known to be sintered with a liquid phase such that possible softening of the grain boundary phase might be triggered by the electric field. A clear effect of an electric field on the sintering of alumina with a glassy phase (including a reduction in viscosity) has been shown, so similar behavior is expected for fully dense samples under mechanical loading (111). Grain boundary amorphization was observed in SiAlON ceramics processed under an electric field (**Figure 8*c***). The sintering aids were segregated to the grain boundary, which melted due to the high current density, resulting in an amorphous intergranular film leading to enhanced plasticity (102).

3.2.5. Role of dislocations.

Dislocation motion is paramount to the plasticity of any material. The application of an electric field may cause Joule heating, which results in an enhanced dislocation mobility at high temperatures. However, the dislocations in ionic crystals have charged cores, which give rise to an electrostatic field that is susceptible to an externally applied electric field (112). Moreover, electric fields have also been observed to create partial dislocations in a ferroelectric oxide by providing the activation energy for the cation to flip to a new metastable configuration (113). The analysis of electric field–enhanced dislocation mobility toward plasticity is complex for submicron-grained ceramics. Li et al. (114) showed that the dislocations in a zinc sulfide single crystal can move back and forth in the presence of an electric field with corresponding polarities without any mechanical loading. An AC field would consequently allow the charged dislocation to be stationary with the polarity reversal (94). On the other hand, plasticity in ceramics might be triggered even in the presence of a noncontacting electric field.

Dislocation motion can be the rate-controlling mechanism, for example, during grain boundary sliding (92), and can be affected by electric fields (115–117). Electric fields can indeed indirectly (by inducing high heating and cooling rates) or directly modify the microstructure and induce 2D defects such as dislocations and stacking faults. Liu et al. (74) showed that zirconia samples displayed dislocation arrays and entanglement when deformed at a current density of 220 mA/mm^2, whereas a lower current did not result in any dislocation, proving that the electric current was the reason for dislocation generation (**Figure 8*d***).

The microstructure of flash-sintered ceramics is modified, with a higher number of stacking faults and dislocations, as shown in **Figure 8*e*** (87). The dislocation density in many grains reaches as high as $\sim 2\text{–}3 \times 10^{12}\ m^{-2}$, compared with the typical density of $\sim 10^8\text{–}10^{10}\ m^{-2}$ in most ceramics. These high-density dislocations play a vital role in the deformability of the flash-sintered 3YSZ tested at elevated temperatures. Interactions between dislocations and with point defects may be affected by chemistry or by thermochemical or electrochemical reduction processes. For example, the increase in oxygen vacancy concentration after reduction treatment was found to significantly influence dislocation-governed plasticity by favoring dislocation nucleation but impeding dislocation motion in STO crystals (118).

4. CONCLUSION

A spectrum of electroplasticity investigations of both ceramics and metals are covered in this review in a structured manner. The mechanisms leading to the deformation of ceramics and metals in the presence of an electric field are very different. The complex mechanisms leading to electroplasticity in metals have been understood with advanced characterization and modeling techniques. Depending on the materials and electric loading conditions (especially current density), the contributions of the different mechanisms (electron wind force, electrostatic force, pinch and surface effects, magnetic force, etc.) on dislocation motion and microstructure have been shown.

Electroplasticity in ceramics is less complex, and a clear athermal effect of an electric field on anelastic deformation has been established. Nonequilibrium, atomistic structural changes in

Downloaded from www.annualreviews.org. Helmholtz Association (ar-410296) IP: 134.94.123.71 On: Mon, 10 Aug 2026 17:14:48

grain boundaries induced by an electric field play a key role in the electroplasticity of ceramics. In particular, the introduction of a high concentration of oxygen defects has been pointed out not only by the abovementioned studies but also by several reports on flash sintering (119, 120). In order to understand the electroplasticity mechanism of ceramics, it is necessary to clarify the relationship between GBS, atomic diffusion, and dislocation motion and the grain boundary structures under an electric field. For this purpose, theoretical approaches, such as thermodynamic (120) and first-principle calculations (121) of the interaction between an electric field or current and the grain boundary, are expected to be very effective. At low temperatures, the high dislocation density induced in flash-sintered ceramics may have general implications for improving the plasticity of sintered ceramic materials.

Electroplasticity in both ceramics and metals offers avenues to achieve material–property processing, which has conventionally not been possible. Electroplasticity may be the answer to certain machinability limitations for engineering ceramics, metals, and metal–ceramic composites.

DISCLOSURE STATEMENT

The authors are not aware of any affiliations, memberships, funding, or financial holdings that might be perceived as affecting the objectivity of this review.

ACKNOWLEDGMENTS

Financial support within the Deutsche Forschungsgemeinschaft priority program Fields Matter (SPP 1959) is greatly acknowledged. S.-K.L. and Y.-C.L. greatly appreciate the financial support from the National Science and Technology Council of Taiwan through projects C112-2622-8-006-020 and 112-2628-E-006-019. H.N.H. appreciates the financial support from the National Research Foundation of Korea grant NRF-2021R1A2C3005096.

LITERATURE CITED

1. Conrad H. 2000. Electroplasticity in metals and ceramics. *Mater. Sci. Eng. A* 287(2):276–87
2. Troitskij OA, Spitsyn VI, Moiseenko MM. 1987. Electroplastic deformation of tungsten. *Dokl. Akad. Nauk SSSR* 295(5):1114–18
3. Mutovin VD, Klimov KM, Trakhoniotovskaya OV, Nefedov VI, Novikov II, et al. 1978. Fabrication of tungsten strip by electroplastic rolling of wire. *Izv. Akad. Nauk SSSR Metall.* 4:125–29
4. Xu Z, Tang G, Tian S, Ding F, Tian H. 2007. Research of electroplastic rolling of AZ31 Mg alloy strip. *J. Mater. Process. Technol.* 182(1–3):128–33
5. Troitskii O, Likhtman V. 1963. The anisotropy of the action of electron and radiation on the deformation of zinc single crystal in the brittle state. *Dokl. Akad. Nauk SSSR* 148:332–34
6. Liu J, Jia D, Fu Y, Kong X, Lv Z, et al. 2024. Electroplasticity effects: from mechanism to application. *Int. J. Adv. Manuf. Technol.* 131(5–6):3267–86
7. Dimitrov NK, Liu Y, Horstemeyer MF. 2022. Electroplasticity: a review of mechanisms in electro-mechanical coupling of ductile metals. *Mech. Adv. Mater. Struct.* 29(5):705–16
8. Stolyarov V, Misochenko A. 2023. A pulsed current application to the deformation processing of materials. *Materials* 16(18):6270
9. Conrad H, Sprecher AF. 1989. The electroplastic effect in metals. In *Dislocations in Solids*, Vol. 8, ed. FRN Nabarro, pp. 498–541. Amsterdam: Elsevier
10. Conrad H, Sprecher AF, Mannan SL. 1985. The electroplastic effect in metals. In *The Mechanics of Dislocations*, ed. EC Aifantis, JP Hirth, pp. 225–36. Metals Park, OH: Am. Soc. Metals
11. Gerstein G, Körkemeyer F, Dalinger A, Zaefferer S, Maier HJ. 2019. Anomalous twinning in AZ 31 magnesium alloy during electrically assisted forming. *Mater. Lett.* 255:126516
12. Valek BC, Tamura N, Spolenak R, Caldwell WA, MacDowell AA, et al. 2003. Early stage of plastic deformation in thin films undergoing electromigration. *J. Appl. Phys.* 94(6):3757–61

Downloaded from www.annualreviews.org. Helmholtz Association (ar-410296) IP: 134.94.123.71 On: Mon, 10 Aug 2026 17:14:48

13. Zhao S, Zhang R, Chong Y, Li X, Abu-Odeh A, et al. 2020. Defect reconfiguration in a Ti–Al alloy via electroplasticity. *Nat. Mater.* 20:468–72
14. Liu YC, Lin SK, Chiu SJ. 2020. On the Schmid's Law for the electric current-induced deformation: an in situ EBSD study. *Int. J. Mech. Sci.* 168:105295
15. Conrad H, Karam N, Mannan S. 1984. Effect of prior cold work on the influence of electric current pulses on the recrystallization of copper. *Scr. Metall.* 18(3):275–80
16. Liu YC, Yu YS, Lin SK, Chiu S-J. 2019. Electromigration effect upon single- and two-phase Ag-Cu alloy strips: an in situ study. *Scr. Mater.* 173:134–38
17. Conrad H, Karam N, Mannan S, Sprecher AF. 1988. Effect of electric current pulses on the recrystallization kinetics of copper. *Scr. Metall.* 22(2):235–38
18. Lin SK, Yeh CK, Xie W, Liu YC, Yoshimura M. 2013. *Ab initio*-aided CALPHAD thermodynamic modeling of the Sn-Pb binary system under current stressing. *Sci. Rep.* 3(1):2731–84
19. Chiu YT, Lin KL, Lai YS. 2012. Dissolution of Sn in a SnPb solder bump under current stressing. *J. Appl. Phys.* 111(4):043517
20. Kim MJ, Lee MG, Hariharan K, Hong ST, Choi IS, et al. 2017. Electric current–assisted deformation behavior of Al-Mg-Si alloy under uniaxial tension. *Int. J. Plast.* 94:148–70
21. Domínguez-Rodríguez A, Gómez-García D. 2010. Superplasticity in ceramics: accommodation-controlling mechanisms revisited. *Ceram. Sci. Technol.* 2:633–63
22. Salandro WA, Jones JJ, Bunget C, Mears L, Roth JT. 2015. *Electrically Assisted Forming: Modeling and Control*. Cham, Switz.: Springer
23. Kravchenko VY. 1967. Effect of directed electron beam on moving dislocations. *ZhETF* 51:1676–81
24. Troitskii OA. 1969. Electromechanical effect in metals. *ZhETF Pisma Redaktsiiu* 10:18–22
25. Kim MJ, Yoon S, Park S, Jeong HJ, Park JW, et al. 2020. Elucidating the origin of electroplasticity in metallic materials. *Appl. Mater. Today* 21:100874
26. Li X, Turner J, Bustillo K, Minor AM. 2022. In situ transmission electron microscopy investigation of electroplasticity in single crystal nickel. *Acta Mater*. 223:117461
27. Krishnaswamy H, Kim MJ, Hong S-T, Kim D, Song J-H, et al. 2017. Electroplastic behaviour in an aluminium alloy and dislocation density based modelling. *Mater. Des.* 124:131–42
28. Andre D, Burlet T, Körkemeyer F, Gerstein G, Gibson JSK-L, et al. 2019. Investigation of the electroplastic effect using nanoindentation. *Mater. Des.* 183:108153
29. Krishnaswamy H, Tiwari J, Amirthalingam M. 2024. Revisiting electron-wind effect for electroplasticity: a critical interpretation. *Vacuum* 221:112937
30. Lahiri A, Shanthraj P, Roters F. 2019. Understanding the mechanisms of electroplasticity from a crystal plasticity perspective. *Model. Simul. Mater. Sci. Eng.* 27(8):085006
31. Grimm TJ, Mears LM. 2022. Skin effects in electrically assisted manufacturing. *Manuf. Lett.* 34:67–70
32. Jeong HJ, Kim MJ, Choi SJ, Park JW, Choi H, et al. 2020. Microstructure reset-based self-healing method using sub-second electric pulsing for metallic materials. *Appl. Mater. Today* 20:100755
33. Huang T, Yang F, Xing B-H, Song K-X, Xiang N, et al. 2024. Effects of electrical pulse on metal deformation behaviors. *Mater. Res. Express* 11(3):032003
34. Vdovin EE, Kasumov AU. 1988. Direct observation of electrotransport of dislocations in a metal. *Sov. Phys. Solid State* 30(1):180–81
35. Nabarro FRN. 1967. *The Theory of Crystal Dislocations*. London: Oxford Univ. Press
36. Klimov KM, Shnyrev GD, Novikov II. 1974. On the electroplasticity of metals. *Dokl. Akad. Nauk SSSR* 219(2):323–24
37. Fiks V. 1981. Interaction of conduction electrons with single dislocations in metals. *Sov. J. Exp. Theor. Phys.* 53(6):1209–11
38. Tiwari J, Balaji V, Krishnaswamy H, Amirthalingam M. 2022. Dislocation density based modelling of electrically assisted deformation process by finite element approach. *Int. J. Mech. Sci.* 227:107433
39. Tiwari J, Pratheesh P, Bembalge OB, Krishnaswamy H, Amirthalingam M, Panigrahi SK. 2021. Microstructure dependent electroplastic effect in AA 6063 alloy and its nanocomposites. *J. Mater. Res. Technol.* 12:2185–204
40. Dubinko VI, Klepikov VF. 2008. Kinetic mechanism of the electroplastic effect in metals. *Bull. Russ. Acad. Sci. Phys.* 72(9):1188–89

Downloaded from www.annualreviews.org. Helmholtz Association (ar-410296) IP: 134.94.123.71 On: Mon, 10 Aug 2026 17:14:48

41. Alers GA, Buck O, Tittmann BR. 1969. Measurements of plastic flow in superconductors and the electron-dislocation interaction. *Phys. Rev. Lett.* 23(6):290–93
42. Jeong K, Jin S-W, Kang S-G, Park J-W, Jeong H-J, et al. 2022. Athermally enhanced recrystallization kinetics of ultra-low carbon steel via electric current treatment. *Acta Mater*. 232:117925
43. Waryoba D, Islam Z, Wang B, Haque A. 2019. Low temperature annealing of metals with electrical wind force effects. *J. Mater. Sci. Technol.* 35(4):465–72
44. Molotskii M, Fleurov V. 1995. Magnetic effects in electroplasticity of metals. *Phys. Rev. B* 52(22):15829–34
45. Klimov KM, Novikov II. 1984. The "electroplastic effect." *Strength Mater*. 16(2):270–76
46. Sprecher AF, Mannan SL, Conrad H. 1986. Overview no. 49: on the mechanisms for the electroplastic effect in metals. *Acta Metall.* 34(7):1145–62
47. Sediako DG, Kasprzak W, Czerwinski F, Nabawy AM, Farkoosh AR. 2016. High temperature creep evolution in Al-Si alloys developed for automotive powertrain applications: a neutron in-situ study on *hkl*-plane creep response. In *Light Metals 2016*, ed. E Williams, pp. 131–36. Cham, Switz.: Springer
48. Sutton AP, Todorov TN. 2021. Theory of electroplasticity based on electromagnetic induction. *Phys. Rev. Mater.* 5(11):113605
49. Molotskii MI. 1991. Possible mechanism of the magnetoplastic effect. *Sov. Phys. Solid State* 33(10):1760–61
50. Becker KP. 2000. *Kurzzeitspeicher mit Doppelschichtkondensatoren zur Stützung von Gleichspannungszwischenkreisen*. PhD Thesis, Universität Karlsruhe, Karlsruhe, Ger.
51. Liu Y, Lin S. 2019. A critical review on the electromigration effect, the electroplastic effect, and perspectives on the effects of electric current upon alloy phase stability. *JOM* 71(9):3094–106
52. Blech IA. 1976. Electromigration in thin aluminum films on titanium nitride. *J. Appl. Phys.* 47(4):1203–8
53. Tu KN. 2003. Recent advances on electromigration in very-large-scale-integration of interconnects. *J. Appl. Phys.* 94(9):5451–73
54. Liang CL, Lee SW, Lin KL. 2017. The mechanism of an increase in electrical resistance in Al thin film induced by current stressing. *Thin Solid Films* 636:164–70
55. Frankovic R, Bernstein GH, Clement JJ. 1996. Pulsed-current duty cycle dependence of electromigration-induced stress generation in aluminum conductors. *IEEE Electron. Device Lett.* 17(5):244–46
56. Fillippi RG, Biery GA, Wood MH. 1993. Evidence of the electromigration short-length effect in aluminum-based metallurgy with tungsten diffusion barriers. *MRS Online Proc. Libr.* 309:141–48
57. Perkins TA, Kronenberger TJ, Roth JT. 2007. Metallic forging using electrical flow as an alternative to warm/hot working. *J. Manuf. Sci. Eng.* 129(1):84–94
58. Frankovic R, Bernstein GH. 1996. Electromigration drift and threshold in Cu thin-film interconnects. *IEEE Trans. Electron. Devices* 43(12):2233–39
59. Ney D, Federspiel X, Girault V, Thomas O, Gergaud P. 2006. Stress-induced electromigration backflow effect in copper interconnects. *IEEE Trans. Electron. Device Mater. Reliab.* 6(2):175–80
60. Arnaud L, Berger T, Reimbold G. 2003. Evidence of grain-boundary versus interface diffusion in electromigration experiments in copper damascene interconnects. *J. Appl. Phys.* 93(1):192–204
61. Chai Y, Chan PCH, Fu Y, Chuang YC, Liu CY. 2008. Electromigration studies of Cu/carbon nanotube composite interconnects using Blech structure. *IEEE Electron. Device Lett.* 29(9):1001–3
62. Ogawa ET, Bierwag AJ, Lee KD, Matsuhashi H, Justison PR, et al. 2001. Direct observation of a critical length effect in dual-damascene Cu/oxide interconnects. *Appl. Phys. Lett.* 78(18):2652–54
63. Wang PC, Filippi RG. 2001. Electromigration threshold in copper interconnects. *Appl. Phys. Lett.* 78(23):3598–600
64. Chiu YT, Liu CH, Lin KL, Lai YS. 2011. Supersaturation induced by current stressing. *Scr. Mater.* 65(7):615–17
65. Wei CC, Liu CY. 2005. Electromigration studies of Sn(Cu) and Sn(Ni) alloy stripes. *J. Mater. Res.* 20(8):2072–79
66. Li Y, Goyal D, eds. 2017. *3D Microelectronic Packaging: From Fundamentals to Applications*. Cham, Switz.: Springer

Downloaded from www.annualreviews.org. Helmholtz Association (ar-410296) IP: 134.94.123.71 On: Mon, 10 Aug 2026 17:14:48

67. Salandro WA, Bunget C, Mears L. 2011. Electroplastic modeling of bending stainless steel sheet metal using energy methods. *J. Manuf. Sci. Eng.* 133(4):041008
68. Magargee J, Morestin F, Cao J. 2013. Characterization of flow stress for commercially pure titanium subjected to electrically assisted deformation. *J. Eng. Mater. Technol.* 135(4):041003
69. Mitchell TE. 2013. Dislocations in ceramics. *Ceram. Sci. Technol.* 2–4:379–436
70. Langdon TG. 2006. Grain boundary sliding revisited: developments in sliding over four decades. *J. Mater. Sci.* 41(3):597–609
71. Wakai F, Sakaguchi S, Matsuno Y. 1986. Superplasticity of yttria-stabilized tetragonal ZrO_2 polycrystals. *Adv. Ceram. Mater.* 1:259–63
72. Porz L, Klomp AJ, Fang X, Li N, Yildirim C, et al. 2021. Dislocation-toughened ceramics. *Mater. Horiz.* 8(5):1528–37
73. Neiman AS, Rothwell WS. 1963. Effect of an electric field on creep of MgO single crystals. *Appl. Phys. Lett.* 3(9):160–61
74. Liu D, Wang K, Zhao K, Liu J, An L. 2022. Creep behavior of zirconia ceramics under a strong DC field. *Scr. Mater.* 214:114654
75. Cologna M, Rashkova B, Raj R. 2010. Flash sintering of nanograin zirconia in <5 s at 850°C. *J. Am. Ceram. Soc.* 93(11):3556–59
76. Yoshida H, Sasaki Y. 2018. Low temperature and high strain rate superplastic flow in structural ceramics induced by strong electric-field. *Scr. Mater.* 146:173–77
77. M'Peko J-C, Francis JSC, Raj R. 2013. Impedance spectroscopy and dielectric properties of flash versus conventionally sintered yttria-doped zirconia electroceramics viewed at the microstructural level. *J. Am. Ceram. Soc.* 96(12):3760–67
78. Conrad H, Yang D. 2000. Influence of an electric field on the plastic deformation of fine-grained MgO at high homologous temperatures. *Acta Mater*. 48(16):4045–52
79. Yang D, Conrad H. 2008. Retardation of grain growth and cavitation by an electric field during superplastic deformation of ultrafine-grained 3Y-TZP at 1,450–1,600°C. *J. Mater. Sci.* 43(13):4475–82
80. Petrenko VF, Schulson EM. 1993. Action of electric fields on the plastic deformation of pure and doped ice single crystals. *Philos. Mag. A* 67(1):173–85
81. Motomura H, Tamao D, Nambu K, Masuda H, Yoshida H. 2022. Athermal effect of flash event on high-temperature plastic deformation in Y_2O_3-stabilized tetragonal ZrO_2 polycrystal. *J. Eur. Ceram. Soc.* 42(12):5045–52
82. Cao C, Mücke R, Guillon O. 2020. Effect of AC field on uniaxial viscosity and sintering stress of ceria. *Acta Mater*. 182:77–86
83. Masuda H, Morita K, Tokunaga T, Yamamoto T, Yoshida H. 2022. Anelasticity induced by AC flash processing of cubic zirconia. *Acta Mater*. 227:117704
84. Cao C, Mücke R, Wakai F, Guillon O. 2020. Viscous Poisson's ratio, bulk and shear viscosity during electrical field assisted sintering of polycrystalline ceria. *Scr. Mater.* 178:240–43
85. Wang K, Chen G, Wang Q, Fu X, Zhou W. 2021. Unusual electrode-dependent deformation of 3Y-TZP induced by weak electric current in oxygen-lean atmosphere. *Scr. Mater.* 205:114220
86. Shen Z, Peng H, Nygren M. 2003. Formidable increase in the superplasticity of ceramics in the presence of an electric field. *Adv. Mater.* 15(12):1006–9
87. Cho J, Li Q, Wang H, Fan Z, Li J, et al. 2018. High temperature deformability of ductile flash-sintered ceramics via in-situ compression. *Nat. Commun.* 9(1):2063
88. Owen DM, Chokshi AH. 1998. The high temperature mechanical characteristics of superplastic 3 mol% yttria stabilized zirconia. *Acta Mater*. 46(2):667–79
89. Morita K, Kim BN. 2022. Effect of electric current on high temperature flow behavior of 8Y-CSZ ceramics. *J. Eur. Ceram. Soc.* 42(5):2341–48
90. Sudhir B, Chokshi AH. 2001. Compression creep characteristics of 8-mol%-yttria-stabilized cubic-zirconia. *J. Am. Ceram. Soc.* 84(11):2625–32
91. Motohashi Y, Watanabe K, Ohmori M, Kubota M. 1990. An evaluation method of superplastic properties in ceramics by means of a three-point bend test (comparison of the bend test results with tension test results). *Trans. Jpn. Soc. Mech. Eng. Ser. A* 56(528):1876–84

Downloaded from www.annualreviews.org. Helmholtz Association (ar-410296) IP: 134.94.123.71 On: Mon, 10 Aug 2026 17:14:48

92. Morita K, Hiraga K. 2002. Critical assessment of high-temperature deformation and deformed microstructure in high-purity tetragonal zirconia containing 3 mol.% yttria. *Acta Mater*. 50(5):1075–85
93. Berbon MZ, Langdon TG. 1999. An examination of the flow process in superplastic yttria-stabilized tetragonal zirconia. *Acta Mater*. 47(8):2485–95
94. Dash A, Morita K, Balice L, Mücke R, Guillon O. 2023. Creep and superplasticity of gadolinium doped ceria ceramics under AC electric current. *Adv. Eng. Mater.* 25(18):2300057
95. Kim SW, Kim SG, Jung J-I, Kang SJL, Chen IW. 2011. Enhanced grain boundary mobility in yttria-stabilized cubic zirconia under an electric current. *J. Am. Ceram. Soc.* 94(12):4231–38
96. Todd RI, Zapata-Solvas E, Bonilla RS, Sneddon T, Wilshaw PR. 2015. Electrical characteristics of flash sintering: thermal runaway of Joule heating. *J. Eur. Ceram. Soc.* 35(6):1865–77
97. Raj R. 2012. Joule heating during flash-sintering. *J. Eur. Ceram. Soc.* 32(10):2293–301
98. Yamashita Y, Kurachi T, Tokunaga T, Yoshida H, Yamamoto T. 2020. Blue photo luminescence from 3 mol%Y_2O_3-doped ZrO_2 polycrystals sintered by flash sintering under an alternating current electric field. *J. Eur. Ceram. Soc.* 40(5):2072–76
99. Itoh A, Tokunaga T, Kodaira A, Yoshida H, Yamamoto T. 2022. Variation of photoluminescence intensity depending on the timing of electric field application during isothermal flash sintering for 3mol%Y_2O_3-ZrO_2 polycrystal. *Ceram. Int.* 48(19):28712–17
100. Schmerbauch C, Gonzalez-Julian J, Röder R, Ronning C, Guillon O. 2014. Flash sintering of nanocrystalline zinc oxide and its influence on microstructure and defect formation. *J. Am. Ceram. Soc.* 97(6):1728–35
101. Morisaki N, Yoshida H, Kobayashi T, Tokunaga T, Yamamoto T. 2018. Intergranular amorphous films formed by DC electric field in pure zirconia. *J. Am. Ceram. Soc.* 101(8):3282–87
102. Luo J, Xi C, Gu Y, Zhang L, Zhang C, et al. 2019. Superplastic forging for sialon-based nanocomposite at ultralow temperature in the electric field. *Sci. Rep.* 9(1):2452
103. Qu B, Eiteneer D, Hughes LA, Preusker JH, Wood J, et al. 2023. Defect redistribution along grain boundaries in $SrTiO_3$ by externally applied electric fields. *J. Eur. Ceram. Soc.* 43(4):1625–32
104. Rheinheimer W, Phuah XL, Wang H, Lemke F, Hoffmann MJ, Wang H. 2019. The role of point defects and defect gradients in flash sintering of perovskite oxides. *Acta Mater*. 165:398–408
105. Qin W, Muche DNF, Castro RHR, van Benthem K. 2018. The effect of electric fields on grain growth in $MgAl_2O_4$ spinel. *J. Eur. Ceram. Soc.* 38(16):5512–18
106. Chaim R. 2019. On the kinetics of liquid-assisted densification during flash sintering of ceramic nanoparticles. *Scr. Mater.* 158:88–90
107. Yoshimura M, Kaneko M, Sōmiya S. 1986. Rapid quenching of melts in the system ZrO_2-SiO_2-Al_2O_3. *J. Phys. Colloq*. 47:473–77
108. Hayakawa M, Onda Y, Oka M, Yoshimura M, Yashima M. 1993. Electron microscopic observation of rapidly cooled ZrO_2-3 mol % Sm_20_3 from the melt. *J. Mater. Sci.* 28:6066–69
109. Samae V, Cordier P, Demouchy S, Bollinger C, Gasc J, et al. 2021. Stress-induced amorphization triggers deformation in the lithospheric mantle. *Nature* 591(7848):82–86
110. Morita K, Naito F, Terada D. 2021. Microcrack healing in zirconia ceramics under a DC electric field/current. *J. Eur. Ceram. Soc.* 41(16):282–89
111. Gonzalez-Julian J, Guillon O. 2015. Effect of electric field/current on liquid phase sintering. *J. Am. Ceram. Soc.* 98(7):2018–27
112. Whitworth RW. 1975. Charged dislocations in ionic crystals. *Adv. Phys.* 24(2):203–304
113. Evans DM, Småbråten DR, Holstad TS, Vullum PE, Mosberg AB, et al. 2021. Observation of electric-field-induced structural dislocations in a ferroelectric oxide. *Nano Lett*. 21(8):3386–92
114. Li M, Shen Y, Luo K, An Q, Gao P, et al. 2023. Harnessing dislocation motion using an electric field. *Nat. Mater.* 22(8):958–63
115. Conrad H. 2001. Space charge and the dependence of the flow stress of ceramics on an applied electric field. *Scr. Mater.* 44(2):311–16
116. Jamnik J, Raj R. 1996. Space-charge-controlled diffusional creep: volume diffusion case. *J. Am. Ceram. Soc.* 79(1):193–98
117. Pannikkat AK, Raj R. 1999. Measurement of an electrical potential induced by normal stress applied to the interface of an ionic material at elevated temperatures. *Acta Mater*. 47(12):3423–31

Downloaded from www.annualreviews.org. Helmholtz Association (ar-410296) IP: 134.94.123.71 On: Mon, 10 Aug 2026 17:14:48

118. Stich S, Ding K, Muhammad QK, Porz L, Minnert C, et al. 2022. Room-temperature dislocation plasticity in $SrTiO_3$ tuned by defect chemistry. *J. Am. Ceram. Soc.* 105(2):1318–29
119. Lebrun JM, Morrissey TG, Francis JSC, Seymour KC, Kriven WM, Raj R. 2015. Emergence and extinction of a new phase during on-off experiments related to flash sintering of 3YSZ. *J. Am. Ceram. Soc.* 98(5):1493–97
120. Charalambous H, Jha SK, Okasinski JS, Tsakalakos T. 2021. Generation of electric-field stabilized zirconium monoxide secondary phase within cubic zirconia. *Scr. Mater.* 190:22–26
121. Dwedari M, Brendel L, Wolf DE. 2022. Non-equilibrium phonon distribution caused by an electrical current. *New J. Phys.* 24(11):113039

Downloaded from www.annualreviews.org. Helmholtz Association (ar-410296) IP: 134.94.123.71 On: Mon, 10 Aug 2026 17:14:48